ACS Catalysis

Research Article

pubs.acs.org/acscatalysis

Mesoporus MCM-22 Zeolites Prepared through Organic Amine-Assisted Reversible Structural Change and Protective Desilication for Catalysis of Bulky Molecules

Yong-Jun Ji,[†] Hao Xu,[†] Da-Rui Wang, Le Xu, Peng Ji, Haihong Wu, and Peng Wu*

Shanghai Key Laboratory of Green Chemistry and Chemical Processes, Department of Chemistry, East China Normal University, North Zhongshan Rd. 3663, Shanghai 200062, People's Republic of China

Supporting Information

ABSTRACT: Mesoporous MCM-22 zeolite (meso-MCM-22) has been prepared by treating MCM-22 with sodium hydroxide solution through an organic amine-assisted reversible structural change. The alkaline treatment conditions, such as temperature, time, organic amine type, and its amount, were examined in detail. The desilication with sole NaOH caused an easy collapse of the crystalline structure of MWW topology. In contrast, the NaOH treatment with the coexistence of piperidine introduced mesopores of ~20 nm into the MCM-22 crystals. Meanwhile, the calcined MCM-22 with three-dimensional (3D) MWW crystalline structure was converted to a 2D layered precursor with a well retained framework. The acid sites related to framework aluminum cations were almost intact after mesopore creation, as evidenced by pyridine or ammonia adsorption−desorption and ^{27}Al NMR investigation. In comparison with MCM-22, meso-MCM-22 possessed a larger external surface, which mitigated effectively the steric restrictions to bulky molecules imposed by the intracrystal micropores. Meso-MCM-22 was superior to MCM-22 in the cracking of 1,3,5-triisopropyl benzene as well as the alkylation of benzene with isopropyl alcohol.

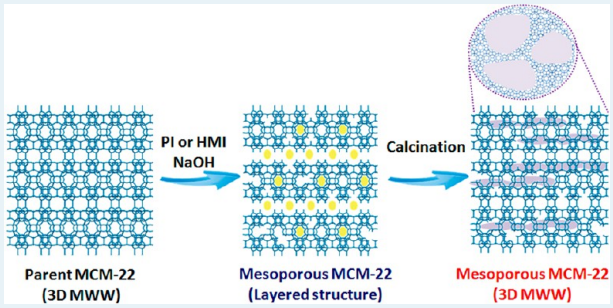

KEYWORDS: *desilication, alkaline treatment, mesoporous zeolites, MCM-22, structural conversion, amine*

1. INTRODUCTION

Zeolite MCM-22, with the MWW topology,[1] is structurally close to aluminosilicates PSH-3[2] and SSZ-25,[3] borosilicate ERB-1,[4] and silicalite ITQ-1.[5] Derived from a lamellar precursor, MCM-22 possesses an unusual crystalline structure consisting of two independent and nonintersecting 10-membered ring (MR) channel systems, that is, intralayer 2D sinusoidal channels and interlayer channels containing 12-MR supercages. Moreover, it possesses 12-MR half cups on the external surface. The unique structure endows MCM-22 with attractive catalytic applications in a variety of reactions. The 10-MR channels within the sheets show unique shape selectivity for reactants and products, and the 12-MR supercages allow bimolecular reactions involving bulky intermediates.[6−9]

With the purpose of applying MCM-22 to petrochemical and fine chemical reactions involving bulky organic molecules, it is desirable to make full use of the acid sites of interlayer supercages and surface pockets. Chu et al. prepared a new microporous mesoporous hybrid material of MCM-36 by swelling and pillaring the MCM-22 lamellar precursor.[10,11] On the other hand, Corma et al. synthesized delaminated ITQ-2 made of MWW thin sheets by treating swollen MCM-22 with ultrasound.[12] Fung et al. synthesized a material of very thin layers denoted as MCM-56, a so-called partially delaminated material characterized by high external surface area and open reaction space.[13] These materials show greatly enhanced activity in acid-catalyzed reactions involving larger molecules, but it is still desirable to find new ways that can eliminate the mass transfer limitation by introducing enlarged pores into MCM-22 bulk crystals.

Alternatively, the mass transfer of molecules can be improved by creating mesopores into the interior of zeolite crystals. The mesopores are formed either by hydrothermal synthesis by using hard or soft templates[14,15] or by postsynthesis means, including dealumination and desilication.[16−18] Featured by inexpensiveness and convenience in comparison to withcostly and complicated direct syntheses, the postsynthesis methods not only introduce mesopores into the zeolites effectively but also cost less. Steaming dealumination is widely used to introduce mesopores into FAU and MOR zeolites.[19,20]

Recently, the desilication by alkaline treatment was proven to be a more effective and simple approach for introducing mesopores into various zeolites, such as MFI,[21] MTW,[22] MOR,[23] BEA,[24] AST,[25] FER,[26] IFR,[27] and STF.[28] Those irregular mesopores are created as a part of silicon atoms are preferentially removed from zeolite crystals by alkaline treatment. Nevertheless, in some cases,

Received: April 15, 2013
Revised: July 6, 2013
Published: July 9, 2013

   dx.doi.org/10.1021/cs400284g | ACS Catal. 2013, 3, 1892−1901

mesopore formation is at the expense of crystalline structure degradation as well as framework Al loss.

Pérez-Ramírez et al. disclosed that the NaOH treatment can introduce efficiently the mesopores with a more uniform and narrower size distribution into ZSM-5 zeolites with well preserved micropores in the presence of quaternary ammonium cations (TPA^+ or TBA^+), as compared with treatment with NaOH only.[29] Their further investigation on the alkaline treatment of pure silica zeolites verified that only when the pore-directing agents were added, such as metal complexes ($Al(OH)_4^-$, $Ga(OH)_4^-$) or quaternary ammonium cations (TPA^+), could the mesopores centered at 5−20 nm be introduced, irrespective of vulnerable siliceous framework.[30] They also pointed out that this kind of protective effect was not observed when using quaternary cations that are able to enter the micropores, for example, TMA^+. The obtained zeolites with a bimodal porosity, that is, micropores and mesopores, showed enhanced catalytic activity, selectivity, and stability for a wide range of reactions, including aromatization,[31] isomerization,[32] alkylation,[23,33] methanol conversion,[34,35] selective oxidation,[36] and hydrodesulfurization[37] as well as medicine and pesticide synthesis reactions involving bulky molecules.[38]

The diffusion transport is expected to be improved if the internal mesopores are introduced into zeolite MCM-22, which would interconnect the sinusoidal intralayer channels and the supercage-containing interlayer channels. Then a three-dimensional pore network is formed, shortcutting the diffusion distance and improving the accessibility of bulky molecules to the active sites within supercages. Xu et al. showed a moderate alkaline treatment on MCM-49 zeolite, an analogue of MCM-22, resulted in an enhanced diffusion of large molecules and, hence, better catalytic performance for liquid-phase alkylation of benzene with ethylene than the parent MCM-49.[39,40] However, considering the fact that the layered structure of MWW zeolites with a pellet morphology does not bear a harsh treatment with NaOH, more effective ways are desirable to increase the surface areas contributed by mesopore formation and then to make full use of the acid sites within supercages.

In this paper, we propose a new route to postsynthesize mesoporous MCM-22 zeolites through a combination of protective desilication and organic amine-assisted reversible structural change, which overcomes shortcomings such as structure collapse that encountered in conventional treatment with NaOH only. The organic amines, originally serving as structure-directing agents for MWW zeolite crystallization, can enter intracrystal micropores to induce 3D-to-2D structural conversion. The resulting materials with well characterized physicochemical properties and structural features are promising catalysts for processing substrates with large molecular dimensions.

2. EXPERIMENTAL SECTION

Material Preparation. Following previously reported procedures,[1] the lamellar precursor of MCM-22 aluminosilicate was hydrothermally synthesized from colloidal silica (30 wt % SiO_2), sodium aluminate (40.52 wt % Na_2O, 53.52 wt % Al_2O_3), sodium hydroxide (96 wt %), deionized water, and hexamethyleneimine (HMI, >98 wt %) as structure-directing agent (SDA). A gel with a molar composition of 1.0 SiO_2/0.0167 Al_2O_3/0.05 Na_2O/0.35 HMI/20 H_2O was crystallized in a Teflon-lined stainless autoclave under rotation (100 rpm) at 423 K for 5 days. The solid product was collected by filtration, washed with deionized water, and dried at 353 K overnight, giving rise to MCM-22 precursor. It was calcined at 823 K for 10 h to obtain MCM-22 with 3D MWW structure.

Mesoporous MCM-22 was postsynthesized by alkaline treatment of directly calcined MCM-22. The alkaline treatment was carried out at a solid-to-liquid weight ratio of 1:50 in 0.1 M NaOH solution at a desirable temperature (338−443 K) for different times (0.25−24 h) in the presence of organic amines including piperidine (PI), HMI, pyridine, piperazine, tetrapropylammonium hydroxide (TPAOH), or tetraethylammonium hydroxide (TEAOH). The amount of added amine or quaternary ammonium corresponded to 0.1−1.0 molar ratio relative to the SiO_2 in zeolite. The sample was collected by filtration; washed with deionized water repeatedly until the pH value reached ∼7; and, finally, dried at 353 K overnight. A subsequent calcination was carried out on the alkaline-treated samples in air at 823 K for 6 h to remove the organic species occluded. The samples thus prepared are denoted as meso-MCM-22. All samples were then ion-exchanged with 1 M NH_4Cl solution three times at 353 K for 2 h. The zeolites were converted into proton form by calcination in air at 823 K for 6 h. For the control experiment, MCM-22 was also treated with NaOH solution using the same procedure but in the absence of any amine or ammonium.

Catalyst Characterizations. The catalysts were characterized by various techniques. X-ray diffraction (XRD) patterns were recorded on a Rigaku Ultima IV X-ray diffractometer (35 kV and 25 mA) using Cu Kα radiation (λ = 1.5405 Å). N_2 adsorption was carried out at 77 K on a BELSORP-MAX instrument after outgassing the samples for 10 h under vacuum at 573 K. The micropore size distribution was determined using the Horvath−Kawazoe (HK) method. The mesopore size distribution was determined by the Barett−Joyner−Halenda (BJH) method from the desorption branches of the isotherms.

The crystal morphology and size were measured by scanning electron microscopy (SEM) on a Hitachi S-4800 microscope. Transmission electron microscopy (TEM) images were collected on a JEOL JEM-2100 microscope operating at an accelerating voltage of 200 kV. The samples were ground, dispersed in ethanol, and deposited on the copper grids prior to observation.

The amount of Si or Al was quantified by inductively coupled plasma (ICP) on a Thermo IRIS Intrepid II XSP atomic emission spectrometer after dissolving the samples in HF solution. TGA-DTG and CHN element analyses were carried out with a Mettler Toledo TGA/SDTA851^e instrument and an Elementar Vario EL analyzer, respectively. The ^{29}Si and ^{27}Al MAS NMR spectra were recorded on a Varian VNMRS 400WB multinuclear solid-state magnetic resonance spectrometer.

Acidity was measured by NH_3-TPD with a Micromeritics tp-5080 apparatus equipped with a thermal conductor detector (TCD). Typically, 100 mg of sample was pretreated in helium stream (30 mL min^{-1}) at 823 K for 1 h. The adsorption of NH_3 was carried out at 323 K for 1 h. The catalyst was flushed with helium at 373 K for 2 h to remove physisorbed NH_3 from the catalyst surface. The TPD profile was recorded at a heating rate of 10 K min^{-1} from 373 to 823 K.

IR spectra were collected on a Nicolet NEXUS-FTIR-670 spectrometer at room temperature. A self-supported wafer (50 mg and Ø 2 cm) was set in a quartz IR cell sealed with CaF_2 windows, where it was evacuated at 673 K for 2 h before the pyridine adsorption. The adsorption was carried out by exposing the wafer to a pyridine vapor (1.3 kPa) at room temperature for 0.5 h. The physisorbed pyridine was then removed by evacuation at 423 K for 1 h. Similarly, the IR

dx.doi.org/10.1021/cs400284g | ACS Catal. 2013, 3, 1892−1901

spectra were measured using 2,6-di-*tert*-butylpyridine as probe molecule to measure the surface acidity of zeolites.

Catalytic Reactions. 1,3,5-Triisopropyl benzene (TIPB) cracking and benzene alkylation with isopropyl alcohol were performed to evaluate the ability of the zeolite catalysts for processing bulky molecules. The reactions were carried out using a continuous flow system in a fixed-bed quartz reactor (i.d., 15 mm) under atmospheric pressure using nitrogen as a carrier gas. The catalyst was activated at 773 K in nitrogen flow (30 mL min^{-1}) for 1.5 h before the reaction. The reactor temperature was then decreased to the reaction temperature, where the reactant was fed into the reactor at a rate of 1.7 mL h^{-1}. The typical catalyst loading and flow rate of nitrogen carrier were 0.2 g and 30 mL min^{-1}, respectively. The liquid products were collected periodically with an ice/water cold trap at 273 K and analyzed on a gas chromatograph (Shimadzu 14B, FID, FFAP capillary column). In poisoning experiments, 2,4-dimethylquinoline (DMQ) was cofed continuously at a rate of 100 μL h^{-1} into the reactor together with the mixture of benzene and isopropyl alcohol or 1,3,5-TIPB.

3. RESULTS AND DISCUSSION

Preparation of Meso-MCM-22 Materials. Figure 1 shows the XRD patterns of MCM-22 and as-treated samples with

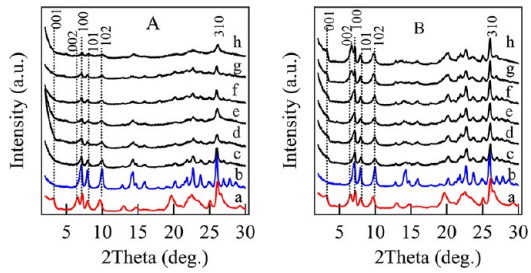

Figure 1. XRD patterns of MCM-22 samples as treated with 0.1 M NaOH solution in the absence of PI (A) and in the presence of PI (B). MCM-22 precursor as-synthesized at Si/Al = 30 (a), directly calcined MCM-22 (b), and the samples obtained by treating calcined MCM-22 at 338 (c), 358 (d), 373 (e), 393 (f), 423 (g), and 443 K (h). The treatment was carried out at a PI/SiO_2 ratio of 1.0 if PI was added.

0.1 M NaOH solution in the absence or presence of PI at various temperatures. The as-synthesized MCM-22 sample showed the characteristic [001] and [002] diffraction peaks in the 2θ region of 3−7° attributed to a layered structure along the *c* direction (Figure 1Aa). In addition, this sample showed two well resolved diffractions due to the [101] and [102] planes, which matched well with the lamellar precursor of MWW topology.[41] When the precursor was subjected to a direct calcination at 823 K for 10 h, the interlayer and intralayer occluded organic species were removed, and the layer-related [001] and [002] reflections almost disappeared or shifted to higher angles as a result of dehydration/condensation of the interlayer hydroxyl groups. Those peaks due to the [h00] and [hk0] indexes, for example, [100] and [310], remained practically unchanged (Figure 1Ab), indicating that the 2D lamellar precursor was transformed to the 3D MWW crystalline zeolite. However, the alkaline treatment with 0.1 M NaOH solution at 338 K for 2 h made MCM-22 with the 3D MWW structure decline in diffraction intensity significantly (Figure 1Ac). The MWW structure-derived diffractions almost disappeared with increasing alkaline treatment temperature, indicating that the cyrstalline structure was destroyed extensively (Figure 1Ad−h). The MCM-22 used in alkaline treatment was synthesized at a Si/Al ratio of 30, which was in the Si/Al ratio region considered suitable for creating mesopores by desilication for other zeolites under similar alkaline treatment conditions.[21,23,42,43] However, with a layered structure and thin platelet morphology (shown below), the MCM-22 crystals tended to be dissolved easily instead of a selective desilication. The 3D MCM-22 zeolite consisting of the collection of MWW sheets is relatively weak in interlayer linkages.[44,45] This kind of delicate structure is assumed to collapse and degrade more easily under harsh alkaline conditions. Thus, to create mesopores within MCM-22 crystals by post modification with NaOH treatment, a protective desilication should be developed to stabilize the MWW structure.

On the other hand, when MCM-22 was treated in 0.1 M NaOH solution at 338 K for 2 h in the presence of PI, the XRD pattern of the resultant sample was very similar to that obtained with NaOH only (Figure 1Bc), indicating structure degradation occurred at this temperature. Nevertheless, the diffraction intensity increased gradually with an increase in the alkaline treatment temperature to 443 K (Figure 1Bd−h). Especially, when the alkaline treatment temperature went up to 423 K, the layered structure-related [001] and [002] peaks were restored in the 2θ region of 3−7° again (Figure 1Bg). In addition, the sample as treated with NaOH in the presence of PI still showed well-resolved diffractions due to the [100], [101], and [102] planes assigned to well-ordered MWW sheets. Continuously increasing alkaline treatment temperature to 443 K, a very similar pattern but with more intensive [001] and [002] diffractions was observed (Figure 1B h). A further calcination at 823 K for 6 h burned off the organic species occluded in the channels and caused an interlayer dehydroxylation. The 3D MWW structure was then restored with the layer-related [001], and [002] diffractions disappeared. The XRD patterns of the calcined samples prepared at 423 and 443 K showed a negligible distinction from that of the parent MCM-22 in diffraction intensity (see Figure S1 in the Supporting Information). The above phenomena indicated that the MWW structure was destroyed easily when MCM-22 was treated with NaOH solution only or even with presence of PI at low temperatures, for example, below 373 K, but it almost stayed intact when treated in the presence of both NaOH and PI at 423 and 443 K. PI was assumed to serve as a protective agent in the process of desilication with NaOH. We once treated Ti−MWW hydrothermally with PI, but in the absence of NaOH with the purpose to enhance its hydrophobicity, and also observed this kind of structure change.[46]

Figure 2 shows the dependence of relative crystallinity of NaOH-treated MCM-22 samples on the alkaline treatment temperature in the absence or presence of PI. Here, the crystallinity of the parent MCM-22 sample was assumed to be 100%. The relative crystallinity was estimated from the intensities of the [100], [101], [102], and [310] reflections. For the NaOH-treated MCM-22 samples prepared in the absence of PI, the relative crystallinity monotonically decreased with increasing alkaline treatment temperature and became only 20% at 443 K (Figure 2a). On the other hand, the crystallinity of the NaOH-treated sample prepared at 338 K in the presence of PI decreased by a large degree compared with that of the parent MCM-22, but afterward, the crystallinity increased continuously at higher alkaline treatment temperatures (Figure 2b). The sample treated at 443 K was comparable to parent MCM-22 in crystallinity, verifying that the coexistence of PI could

dx.doi.org/10.1021/cs400284g | *ACS Catal.* 2013, 3, 1892−1901

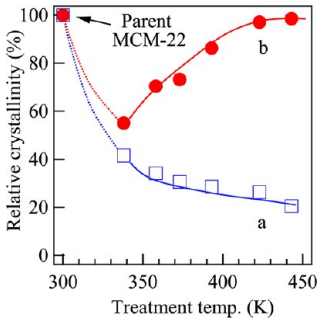

Figure 2. The dependence of relative crystallinity of NaOH-treated MCM-22 samples on the treatment temperature in the absence (a) or presence (b) of PI. The crystallinity was measured from the reflection intensity of the [100], [101], [102], and [310] planes after the NaOH-treated samples were calcined at 823 K.

stabilize the MWW framework against extensive dissolution during alkaline treatment of MCM-22.

The above results showed that MCM-22 with the 3D MWW topology was possibly converted to a 2D MWW layered precursor with the assistance of PI, a typical SDA for crystallizing and constructing the MWW structure. One may be concerned that this phenomenon is just a result of full dissolution of the MCM-22 crystals by NaOH and subsequent renucleation and recrystallization with the assistance of PI. To rule out that the MWW sheets were not destroyed in basic media in the presence of PI, we have thus traced the desilication process in detail, especially at the initial stage. Figure 3 shows the XRD patterns of the samples prepared by

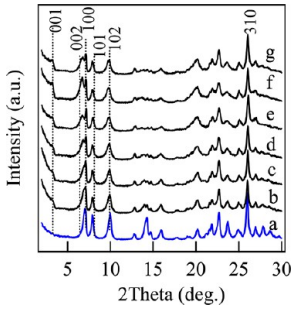

Figure 3. XRD patterns of calcined MCM-22 (Si/Al = 30) (a) and the samples obtained by treating calcined MCM-22 in 0.1 M NaOH solution at PI/SiO_2 of 1.0 and at 443 K for 15 min (b), 40 min (c), 1 h (d), 2 h (e), 8 h (f), and 24 h (g). The NaOH-treated samples were uncalcined.

treating calcined MCM-22 with 0.1 M NaOH solution at a PI/SiO_2 ratio of 1.0 and at 443 K. Within a relatively short alkaline treatment time (15 - 40 min), the obtained samples still showed well-resolved diffractions due to the [100], [101], and [102] planes as a result of the ordered MWW sheets (Figure 3b, c), indicating that a structural degradation did not take place in the solution of NaOH and PI. Although they were still characteristic of the 3D MWW structure, the layer structure-related [001] and [002] diffractions emerged. When the alkaline treatment time was prolonged to 1 h, the [001] and [002] diffractions were obviously developed (Figure 3d), implying that MCM-22 was converted to a 2D layered precursor. The alkaline treatment time did not show any obvious influence on the intensity of [001] and [002] diffractions from 1 to 24 h (Figure 3e–g), indicating the structural change was almost completed within 1 h, and the structural transformation to other phases hardly took place. After calcination at 823 K for 10 h, the layer-related [001] and [002] reflections disappeared or shifted to higher angles as a result of interlayer condensation as the 3D MWW structure was restored (see Figure S2 in the Supporting Information). The diffraction intensity was very comparable during whole desilication process from 15 min to 24 h. These results confirmed that the fundamental structure of the MCM-22 was not destroyed but kept almost intact, even after the alkaline treatment for a prolonged time of 24 h, and also denied the possibility of MCM-22 crystals' dissolving as well as renucleation and recrystallization. It is then deduced that the PI exhibited a kind of protective effect on the MWW framework in the process of desilication.

Using the same parent MCM-22 sample, we further investigated the effect of the amount of PI on desilication and structural conversion. As shown in Figure 4A, the [001] and [002] diffractions due to the layered structure were developed until the PI/SiO_2 molar ratio reached 1.0. At a lower PI/SiO_2 ratio of 0.1, the diffractions decreased slightly (Figure 4Aa). After

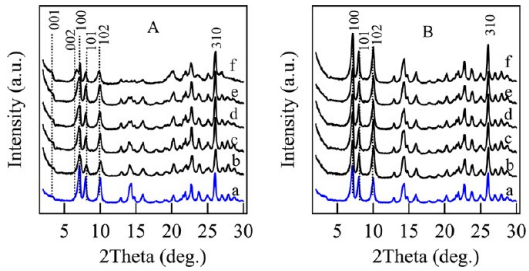

Figure 4. XRD patterns of calcined MCM-22 (Si/Al = 30) (a) and after treatment in 0.1 M NaOH solution at 443 K for 2 h and at PI/SiO_2 ratios of 0.1 (b), 0.3 (c), 0.5 (d), 0.7 (e), and 1.0 (f). The NaOH-treated samples were uncalcined (A) and further calcined at 823 K (B).

calcination at 823 K for 6 h, the 3D MWW structure was restored. The diffractions peaks increased in intensity with increasing PI amount (Figure 4B). Figure S3 shows the dependence of relative crystallinity on the PI/SiO_2 ratio. The crystallinity of NaOH-treated MCM-22 samples increased continuously with increasing PI/SiO_2 molar ratio. This also evidenced that PI played a stabilizing effect on the MWW framework.

To further investigate the effect of the type of amine or quaternary ammonium on the formation of meso-MCM-22, we treated calcined MCM-22 in 0.1 M NaOH solution in the presence of PI, HMI, pyridine, piperazine, TPAOH, or TEAOH. The added amount of amine corresponded to a 1.0 molar ratio relative to SiO_2 in zeolite. Supporting Information Figure S4 shows the XRD patterns of the samples treated at 443 K for 2 h in various organic amines before and after calcination. Similar to PI, treating 3D MWW with NaOH solution in the presence of HMI also led to a structure showing the layered-related [001] and [002] peaks (Supporting Information Figure S4A, c). Further calcination at 823 K for 6 h also made the layered structure convert to a 3D MWW structure, showing the pattern with a comparable intensity to parent MCM-22 (Supporting Information Figure S4B, c). However, when the alkaline treatment was carried out in the presence of pyridine or piperazine, which also possessed cyclic molecular shapes (6 MR) like PI or HMI, a destruction occurred to a certain degree, as evidenced by less-intensive XRD patterns, without a structural conversion to a 2D precursor (Supporting Information Figure S4Ad and e). They showed an obviously different effect from PI and HMI in the

dx.doi.org/10.1021/cs400284g | ACS Catal. 2013, 3, 1892–1901

alkaline treatment of MCM-22 with NaOH solution. The alkaline treatment in the presence of TPAOH or TEAOH made the MWW structure-related diffractions disappear completely while only developing a broad peak at 2θ of 25.9° in the XRD patterns (Supporting Information Figure S4Af and g). The MWW structure was totally destroyed in these strong basic media. Thus, only PI and HMI possessed a stabilizing effect for the MWW structure. Considering the fact that both PI and HMI are capable of serving as SADs in hydrothermal synthesis of MCM-22, in post desilication process, there existed a kind of structural recognition between the guest molecules of organic amines and the host zeolite avoiding structure collapse, which then resulted in a protective desilication.

Characterizations of Meso-MCM-22 Materials. Combining the above experiment results, the conditions used to prepare meso-MCM-22 for following characterizations were as follows: the alkaline treatment was conducted at a solid-to-liquid weight ratio of 1:50 in 0.1 M NaOH solution at 443 K for 2 h in the presence of PI or HMI. The added amount corresponded to a 1.0 molar ratio relative to the SiO_2 in zeolite (for others, see the Experimental Section). Figure 5 shows the

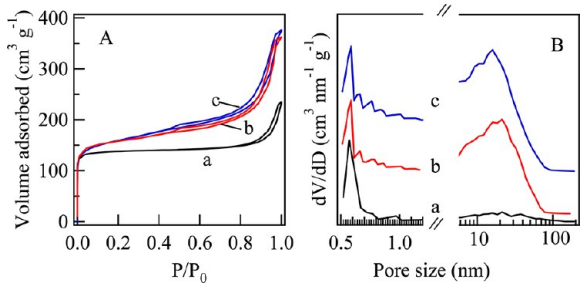

Figure 5. N_2 adsorption and desorption isotherms (A) and pore size distribution (B) of the parent MCM-22 (a), meso-MCM-22 (HMI) (b), and meso-MCM-22(PI) (c).

N_2 adsorption/desorption isotherms of the parent MCM-22 and meso-MCM-22. The parent MCM-22 exhibited a type I isotherm characteristic of microporosity (Figure 6Aa). The meso-MCM-22 sample showed the isotherms featured by both type I and type IV (Figure 5Ab and c), suggesting they contained a hierarchical porous system consisting of micropores and mesopores. The samples as-treated with NaOH solution in the presence of PI and HMI displayed similar isotherms, both of which possessed remarkably increased adsorption capacity as a result of removing a part of the silicon atoms from the framework. The increasing step due to multilayer adsorption in the isotherms at P/P_0 of 0.2−0.4 and the hysteresis loops at P/P_0 of 0.5−0.8 indicated that the mesopores were newly created. Moreover, meso-MCM-22 showed a higher N_2 adsorption at P/P_0 = 0.9−0.99 than the parent MCM-22, implying the possible presence of a more exposed external surface contributed by intercrystal mesopores.

The pore size distribution shows that the parent MCM-22 and meso-MCM-22 displayed a narrow peak near 0.55 nm (Figure 5Ba−c), in accordance with the 10-MR channels of MCM-22, verifying that the desilication did not destroy the structure of the micropores. The introduced mesopores in meso-MCM-22 are centered at around 20 nm (Figure 6Bb and c). On the other hand, the Si/Al ratio decreased from 26 in the parent MCM-22 to 17 in the desilicated sample (Table 1). The mesopore surface area and mesopore volume of the parent MCM-22 (44 $m^2\ g^{-1}$ and 0.15 $cm^3\ g^{-1}$, respectively) increased

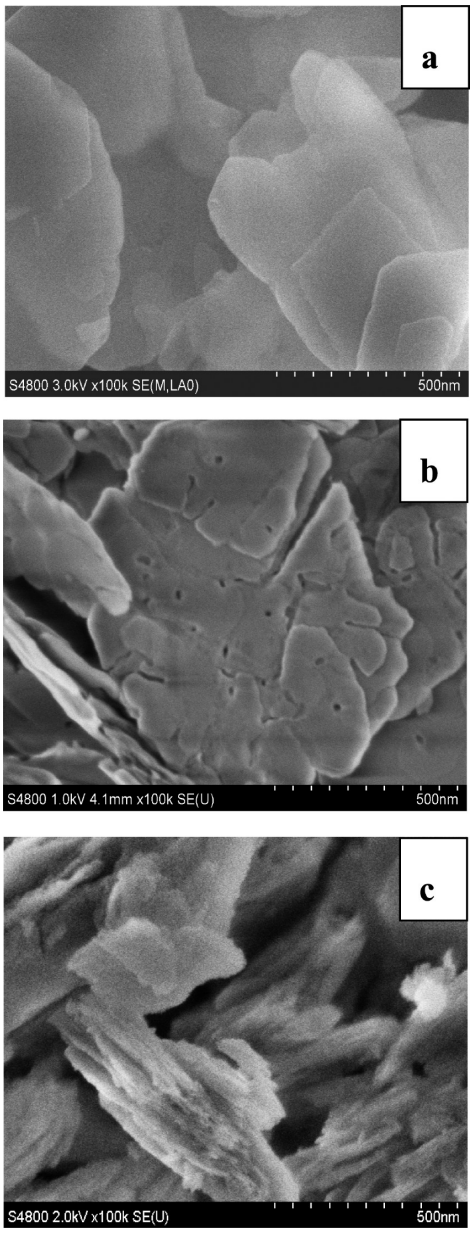

Figure 6. SEM images of MCM-22 (a) and meso-MCM-22 (b) and the samples by treating MCM-22 in 0.1 M NaOH solution at 443 K for 2 h in the absence of amine (c). The amount of quaternary ammonium hydroxide corresponded to 1.0 molar ratio relative to the SiO_2 in zeolite (if added).

to 231−242 $m^2\ g^{-1}$ and 0.38−0.42 $cm^3\ g^{-1}$, respectively, in meso-MCM-22. Meanwhile, the mesopore formation by selective desilication was accompanied by a slight decrease in the micropore volume from 0.17 $cm^3\ g^{-1}$ in parent to 0.15 $cm^3\ g^{-1}$ in the meso-MCM-22. However, the decreased amount of micropore volume was far below the increased amount of the mesopore volume.

The N_2 adsorption/desorption isotherms of the parent MCM-22 and meso-MCM-22 prepared with different alkaline treatment times are depicted in Supporting Information Figure S5. The N_2 uptake did not increase but slightly decreased when the treatment time was prolonged from 2 to 24 h (Supporting Information Figure S5c). This is presumably because the MWW structure was destroyed more after desilication for a longer time.

dx.doi.org/10.1021/cs400284g | ACS Catal. 2013, 3, 1892−1901

Table 1. Textural Properties of the Parent MCM-22 and the NaOH-Treated Samples[a]

samples	Si/Al ratio[b]	surface area (m^2 g^{-1}) S_{BET}[c]	S_{meso}[d]	pore volume (cm^3 g^{-1}) V_{total}[e]	V_{micro}[d]	V_{meso}
MCM-22 (parent)	26	415	44	0.32	0.17	0.15
meso-MCM-22(PI)	17	523	242	0.57	0.15	0.42
meso-MCM-22(HMI)	17	511	231	0.53	0.15	0.38

[a]Calcined MCM-22 was treated in 0.1 M NaOH solution in the presence of PI or HMI (amine/SiO_2 = 1.0) at 443 K for 2 h. [b]Obtained by ICP. [c]Calculated with BET method. [d]Calculated by *t*-plot. [e]Obtained at P/P_0 = 0.99.

Figure 6 shows the SEM images taken with different magnifications for the parent MCM-22 and meso-MCM-22 samples. The parent MCM-22 had a morphology of thin platelets, approximately 0.5−1 μm in length and 0.02−0.05 μm in thickness, and the surface was smooth and distinct (Figure 6a). After being treated in NaOH solution in the presence of PI, both the morphology and the crystal size were intact, but many grooves and voids appeared on the crystal surface of the meso-MCM-22 (Figure 6b). This should be due to dissolving of a part of the silica species from the zeolite crystals in the alkaline treatment. The alkaline corrosion created random voids around 20 nm in size. Nevertheless, the whole crystal shapes were not changed because the MWW structure was well maintained, which was consistent with the results derived from the XRD investigation (Figure 1Bh). On the other hand, the treatment with only the NaOH solution destroyed the crystal platelets severely (Figure 6c), indicating dissolution of the crystals occurred rather than selective desilication. On the other hand, when the MCM-22 was treated with the NaOH solution in the presence of TPAOH or TEAOH, the crystals were dissolved to amorphous materials (see Figure S6 in the Supporting Information).

The TEM images shown in Figure 7 provide more information for the presence of mesopores in meso-MCM-22. Viewed from different crystal surfaces (*ab* and *ac* planes), the parent MCM-22 displayed clear lattice fringes corresponding to the surface 12-MR half cups and 10-MR channels (Figure 7a, b). The lattice fringes were arrayed in a highly ordered manner without any interruption, and the domain contrast of the images also implied that the crystals were almost free of an unconnected region. In particular, the images taken normal to the [001] direction clearly showed the stacking sequence of the MWW sheets was ordered.

In contrast, the TEM images indicated that the crystals of the meso-MCM-22 were abundant in the mesopores, but their size and shape remained almost unaffected (Figure 7c−f). The mesopores newly created by desilication were predominately intracrystal in nature. The high-resolution TEM image taken normal to the *ab* plane showed that the meso-MCM-22 possessed a large number of white spots with 10−50 nm diameters as a result of lattice plane interruption (Figure 7c, e). Along this direction, the mesopores exhibited a side view round or elliptical in shape.

A deep observation indicated that the flat mesopores were formed mainly along the direction of MWW sheet, that is, the *ab* plane (Figure 7e, f). The mesopore positions are indicated by arrows. The growth of mesopores seemed to be terminated along the *c* axis, resulting in a height or thickness that was several times the unit cell parameter, *c*. The mesopores were not sphere-shaped but had a cylinder or coin shape short in

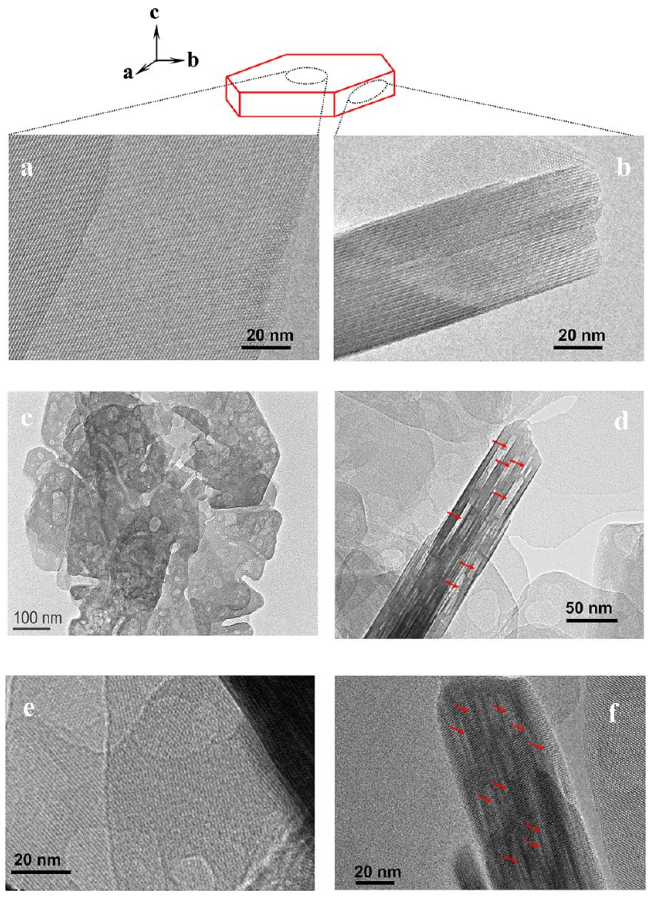

Figure 7. TEM images of MCM-22 (a, b) and meso-MCM-22 (c−f). The arrows indicate the positions of the mesopores.

height and wide in diameter (10−50 nm). Along the *c* direction, the mesopores were formed across several MWW sheets, but their growth was interrupted by the presence of interlayer organic species. Thus, the mesopores were not enlarged equally as those along the *ab* plane, which was probably because the MWW framework was protected by the added PI molecules. The formation of mesopores interrupted the continuity of the original micropore channels, but made two sets of 10-MR channels (interlayer and intralayer) interconnected together. This would reduce the diffusion limitation of the micropores effectively; maximize intracrystal mass transport; and finally, improve the accessibility of the active sites located in the 12-MR supercages.

To investigate the characters of hydroxyl groups and acid sites, the IR spectra in the region of the hydroxyl stretching vibration were measured. As shown in Figure 8a, the parent MCM-22 exhibited the band at 3745 cm^{-1} attributed to isolated silanols, the band at 3725 cm^{-1} probably due to asymmetric hydrogen-bonded internal silanols, and the strong band at 3620 cm^{-1} assigned to structure Si(OH)Al hydroxyls as well as a very weak band around 3663 cm^{-1} due to extraframework aluminum-related hydroxyls.[6] The meso-MCM-22 showed a more intense band at 3745 cm^{-1} but a comparable band at 3620 cm^{-1} (Figure 8b), indicating that most of the framework Al remained intact by desilication. After the adsorption and desorption of pyridine at 423 K, the bands due to the vibration of the pyridine ring were observed (see Figure S7 in the Supporting Information). The bands at 1545 and 1454 cm^{-1} are characteristic of Brønsted and Lewis acid

dx.doi.org/10.1021/cs400284g | *ACS Catal.* 2013, 3, 1892−1901

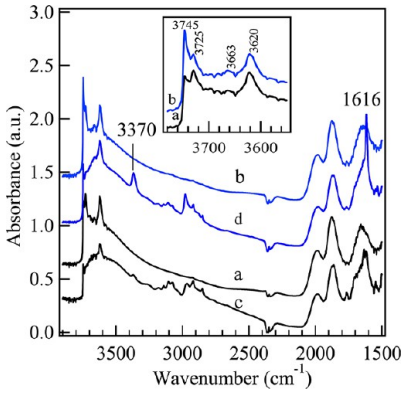

Figure 8. IR spectra of proton-type parent MCM-22 (a, c) and meso-MCM-22 (b, d) before (a, b) and after (c, d) 2,6-di-*tert*-butyl-pyridine adsorption. The inset shows the spectra without 2,6-di-*tert*-butyl-pyridine in the hydroxyl stretching region.

sites, respectively.[6] The 1545 cm^{-1} band was comparable in intensity for meso-MCM-22 and MCM-22, which further suggests the Brønsted acid sites were unaffected by desilication.

The acidic properties of meso-MCM-22 were further characterized using the NH_3-TPD technique. Supporting Information Figure S8 compares its profile with that of the parent MCM-22. The parent MCM-22 sample had two desorption peaks. The former, around 473 K, is assumed to be physically adsorbed ammonia or those adsorbed on weak acid sites, whereas the latter centered at 673 K is the contribution of the ammonia adsorbed on strong acid sites.[47] Compared with MCM-22, the meso-MCM-22 did not show any change in temperature and peak area for the desorption corresponding to strong acid sites, indicating that neither the strength nor the amount of the acid sites changed after desilication. However, the weak acid sites, corresponding to the desorption around 473 K, increased slightly. This is probably because the extraframework Al species increased slightly as the Si/Al ratio decreased from 26 to 17 by NaOH treatment, as shown in Table 1.

The development of external silanols by alkaline treatment was further investigated by ^{29}Si MAS NMR spectroscopy (Figure 9A). The two spectra matched well with those reported

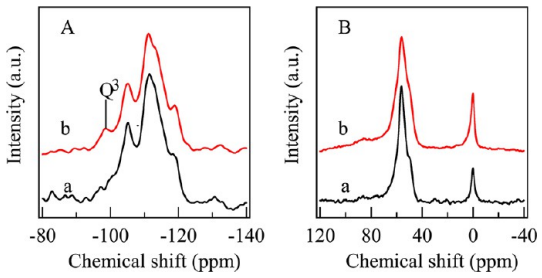

Figure 9. ^{29}Si (A) and ^{27}Al MAS NMR (B) spectra of MCM-22 (a) and meso-MCM-22 (b).

previously for MCM-22. The Q^4 sites in the region of −103 to −120 ppm could be deconvoluted into at least five lines, which are assigned to several distinctive crystallographic sites but with overlapping resonances.[48,49] Compared with parent MCM-22, meso-MCM-22 showed a more obvious intensive resonance around −100 ppm, which is assigned to the Q^3 sites, such as $Si(OH)(SiO)_3$ and $Si(OAl)(SiO)_3$ (Figure 9Ab). Because the alkaline treatment caused a partial removal of Si atoms (Table 1), the −100 ppm resonance is considered to originate from the $Si(OH)(SiO)_3$ groups. This is in agreement with the above IR spectra, verifying the presence of more silanol groups in meso-MCM-22. The ^{27}Al MAS NMR spectra of MCM-22 (Figure 9Ba) clearly showed two sets of signals: a broader band with a maximum at 55 ppm due to tetrahedrally coordinated framework Al and a weak-frequency signal around 0 ppm, which is attributed to octahedral extraframework Al species formed by calcination.[50] Compared with MCM-22, meso-MCM-22 showed no significant change for the tetrahedral framework Al, but the octahedral extraframework Al increased in amount as a result of partial dealumination (Figure 9Bb).

2,6-Di-*tert*-butyl-pyridine (2,6-DTBPy), with a molecular dimension too large to penetrate through the micropores of zeolites, is reported to be chemisorbed only on the external acid sites.[51] DTBPy-IR spectra are thus useful for evaluating the Brønsted acidity on the surface of zeolite crystallites. The adsorption with 2,6-DTBPy for MCM-22 made the bridging hydroxyl groups at 3620 cm^{-1} band almost intact but developed two characteristic bands at 3370 and 1616 cm^{-1} (Figure 8c), which are assigned to the N−H stretching vibration in $DTBPyH^+$ and corresponding ring vibration mode.[51]They are taken as the presence of strong Brønsted acid sites on the crystallite surface of MCM-22. However, the adsorption of 2,6-DTBPy on meso-MCM-22 made the 3370 and 1616 cm^{-1} bands more intensive than MCM-22 (Figure 8d). Evidently, meso-MCM-22 had more Brønsted acid sites accessible to large amine molecules than MCM-22.

To make clear the mechanism of the formation of meso-MCM-22, it is necessary to know the positions of the inserted PI or HMI molecules. Thus, the as-made samples obtained were characterized by thermal analysis. Supporting Information Figure S9 shows TGA and DTG curves of all these samples. The DTG curves implied four kinds of desorption temperature-dependent weight loss (Supporting Information Figure S9B). The weight loss below 473 K is attributed to physisorbed water, whereas the weight loss in the range of 473−643 K is mainly due to the oxidative decomposition of organic species occluded in interlayer void spaces, but in a higher temperature region of 643−873 K, it is ascribed to the removal of organic species from the intralayers of 10-MR sinusoidal channels, and in the range of 873−1073 K, it corresponds to the dehydroxylation.[52,53]

As summarized in Table S1, the organic species had a C/N atomic ratio of 5.7−5.9 for both the precursor and corresponding alkaline-treated sample in the presence of HMI, suggesting that they existed as HMI molecules within the crystals, whereas the organic species had a C/N atomic ratio of 4.9 for the alkaline-treated sample in the presence of PI, suggesting that it existed as PI molecules. The weight loss of the MCM-22 precursor in the interlayer void spaces and in the intralayer 10-MR sinusoidal channels of the precursor was ∼9.3% and 5.3%, respectively. Nevertheless, the weight loss in the interlayer void spaces is more than that in the intralayer 10-MR channels in the alkaline-treated samples in the presence of PI or HMI, indicating that the organic amine molecules preferred to be inserted into the interlayer void spaces. The amount of HMI inserted was slightly lower than that of PI simply because the HMI molecules had a larger molecular dimension than PI.

The above results allow us to describe graphically a possible mechanism for the formation of mesopores through alkaline treatment of 3D MWW MCM-22 with NaOH solution in the presence of PI or HMI (Scheme 1). When the parent MCM-22

Scheme 1. Graphic Description for the Formation of Mesopores within MCM-22 Crystallites by NaOH Treatment in the Presence of PI or HMI

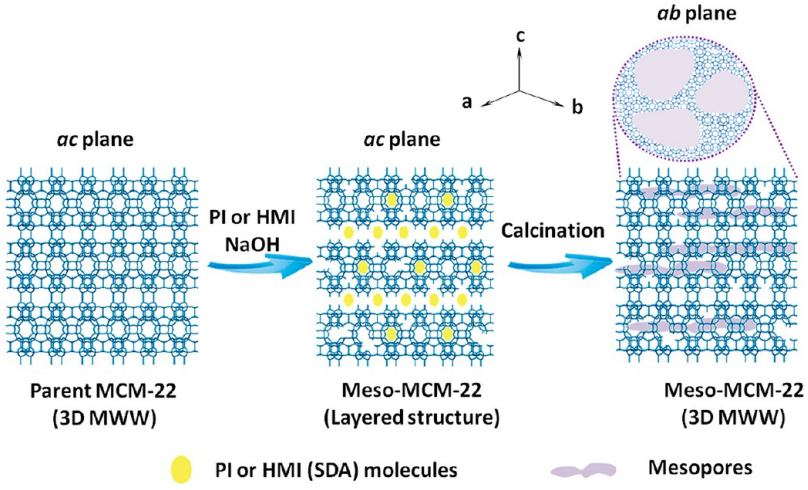

sample was treated with NaOH solution in the presence of amine or organic ammonium, the 3D MWW structure seemed to recognize only PI or HMI molecules at the molecular level. Then the PI molecules were inserted mainly into the interlayer space of MCM-22, which led to a structural conversion into a 2D layered structure.

The TG analysis indicated that the number of PI molecules incorporated into the interlayer space accounted for ~7.3 wt % (Supporting Information Table S1). This amount of organic species would be enough to intercalate the MWW sheets to form the layered structure. Moreover, the PI or HMI molecules were also inserted into the intralayer 10-MR sinusoidal channels. Thus, there existed two organic layers within the *ab* planes. These inserted molecules would stabilize and protect the MWW structure, avoiding an extensive dissolution of the framework along the *c* direction. Then the cylinder-shaped or coin-like mesopores were formed parallel to the MWW sheets within the MCM-22 crystals. A further calcination burned off the occluded organic species and caused an interlayer dehydroxylation, giving rise to mesopore-containing MCM-22 with the 3D MWW topology.

Catalytic Properties of Meso-MCM-22 in Reactions Involving Bulky Molecules. Taking advantage of mesopores, we investigated the catalytic behavior of meso-MCM-22 in a reaction involving substrates with larger molecular sizes because its larger external surface may make the active sites more accessible to the reactants, particularly for bulky molecules.

The cracking of 1,3,5-triisopropylbenzene (TIPB) (0.95 nm diameter) is a convenient model reaction widely used to evaluate the contribution of the external surface area of microporous materials.[54] The main liquid products were diisopropylbenzene (DIPB) isomers, isopropylbenzene (IPB), and benzene (BZ) (Supporting Information Scheme S1). Figure 10A shows the change of the conversion with time on-stream (TOS) in cracking of TIPB. Meso-MCM-22 showed a higher TIPB conversion than MCM-22, although the TIPB conversion decreased with prolonged time for both MCM-22 and meso-MCM-22 catalysts, but obviously, meso-MCM-22 exhibited a slower deactivation rate than MCM-22. Because cracking of TIPB is a successive reaction that yields DIPB, IPB, and BZ, in turn, the product distribution may also reflect the extent of cracking. Figure 10B shows the product distribution in TIPB cracking over MCM-22 and meso-MCM-22 catalysts. With prolonged time, the BZ and IPB selectivities decreased, but the DIPB selectivity increased. This is

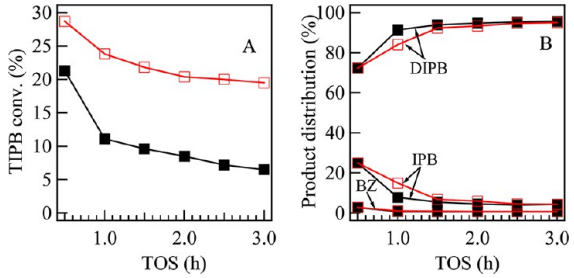

Figure 10. Dependence of TIPB conversion (A) and products selectivity (B) on the MCM-22 (■) and meso-MCM-22 (□) catalysts at different times. Reaction conditions: cat., 0.2 g; feed rate, 1.7 mL h^{-1}; N_2, 30 mL min^{-1}; temp, 573 K; time, 0.5−2.5 h.

as expected because the MWW catalyst easily coked;[6] however, the selectivity for deep cracking products, such as IPB and BZ over meso-MCM-22 catalysts was slightly higher than that of MCM-22 at the same TOS. This indicates that meso-MCM-22 also showed a better cracking ability than MCM-22.

To clarify the role of the external surface in the cracking of TIPB, 2,4-dimethylquinoline (2,4-DMQ), with molecular dimensions too large to enter the pores of 10-MR windows, was adopted to poison selectively the acid sites on the external surface.[55] When the reaction was carried out in the absence of 2,4-DMQ (Figure 11), the TIPB conversion was 11.1% and 23.8% for MCM-22 and meso-MCM-22, respectively. While 2,4-DMQ was cofed into the reactor, the TIPB conversion decreased to a very low level for both catalysts as a result of extinguishing the acid sites on the external surface. This confirmed meso-MCM-22 is advantageous for the reactions of the bulky molecules because it possessed a larger external surface contributed by mesopores.

IPB (cumene) is an important and highly valuable organic chemical raw material in industry that is widely used in producing phenol. As an important reaction for producing IPB, the gas-phase alkylation of benzene with isopropyl alcohol is currently catalyzed by solid-acid catalysts of zeolites. The main liquid product of this reaction was IPB (Supporting Information Scheme S2). Some byproducts, such as DIPB isomers and TIPB, were also produced because of further alkylation of IPB. Figure 12A compares the results of benzene alkylation with isopropyl alcohol between meso-MCM-22 and

dx.doi.org/10.1021/cs400284g | ACS Catal. 2013, 3, 1892−1901

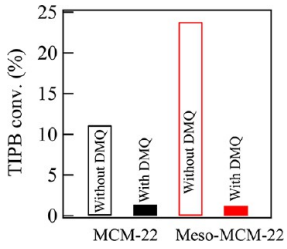

Figure 11. A comparison of TIPB conversion between MCM-22 and meso-MCM-22 in the absence or in the presence of 2,4-DMQ. Reaction conditions: time, 1 h; other conditions, see Figure 4; 2,4-DMQ feed, 100 μL h^{-1}.

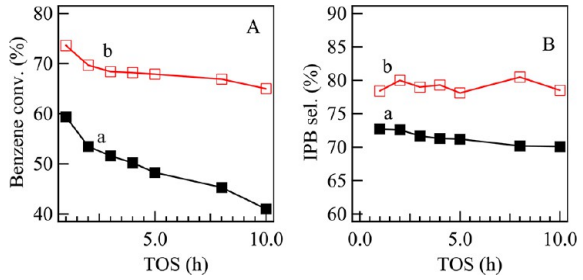

Figure 12. Dependence of benzene conversion (A) and TIPB selectivity (B) on MCM-22 (■) and meso-MCM-22 (□) catalysts at different times. Reaction conditions: cat., 0.2 g; feed rate, 1.7 mL h^{-1}; N_2, 30 mL min^{-1}; temp, 473 K; time, 1−10 h.

MCM-22. The trend was consistent with that of TIPB cracking; that is, the meso-MCM-22 catalyst showed higher benzene conversion than MCM-22, and it also exhibited a much slower deactivation rate. Figure 12B shows the IPB selectivity for MCM-22 and meso-MCM-22 catalysts. The meso-MCM-22 catalyst exhibited much higher IPB selectivity than the MCM-22 catalyst at the same TOS. The IPB product would diffuse out of the zeolite channels more rapidly in the presence of mesopores in meso-MCM-22, which reduced the possibility of side reactions greatly.

Table 2 compares the catalytic activity and product distribution between the MCM-22 and meso-MCM-22

Table 2. Catalytic Activity and Product Distribution in the Gas-Phase Alkylation of Benzene with Isopropyl Alcohol on H-MCM-22 and H-Meso-MCM-22[a]

		product distribution (%)				
catalyst	benzene conv (%)	IPB	DIPBs	TIPB	others	IPBs sel (%)
H-MCM-22	41.0	70.1	23.8	1.3	4.8	95.2
H-meso-MCM-22[b]	65.0	78.5	18.1	0.7	2.7	97.3

[a]Reaction conditions: cat., 0.2 g; temp, 473 K; pressure, 0.1 MPa; benzene/isopropyl alcohol molar ratio, 1.0; feed rate, 1.7 mL h^{-1}; N_2, 30 mL min^{-1}; TOS = 10 h. [b]The catalyst was prepared through treating calcined MCM-22 in 0.1 M NaOH solution at 443 K for 2 h in the presence of PI (PI/SiO_2 = 1.0).

catalysts for the alkylation of benzene with isopropyl alcohol after 10 h. Meso-MCM-22 showed an enhanced benzene conversion and IPB selectivity in comparison with the MCM-22 counterpart. In a commercial process for IPB production, DIPB and TIPB are also regarded as objective products in addition to IPB because they are finally converted into the desirable IPB product through catalytic transalkylation with benzene. Thus, the sum of mono- and poly-IPB is employed to evaluate the catalyst performance. Obviously, the meso-MCM-22 catalyst showed higher isopropylated benzenes (IPBs, including IPB, DIPB, and TIPB) selectivity than MCM-22.

The heavy byproducts were gradually accumulated and deposited inside the channels, which may block the active sites. TG analysis indicated that the used meso-MCM-22 catalyst contained about 9.5 wt % organic species, which showed a weight loss in a wide temperature range (500−850 K). On the other hand, the weight loss corresponding to heavy organic species reached 13.2 wt % on MCM-22 (Figure 13). Thus, the introduced mesopores in meso-MCM-22 catalyst not only

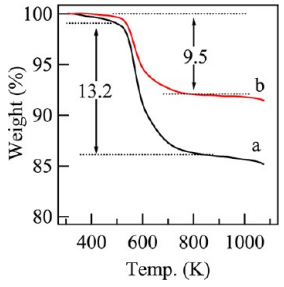

Figure 13. TG curves of MCM-22 (a) and meso-MCM-22 (b) after being used in the alkylation of benzene with isopropyl alcohol for 10 h.

afforded enough space for the diffusion of bulky molecules but also suppressed the coke formation efficiently.

4. CONCLUSIONS

We have successfully prepared meso-MCM-22 zeolite by treating MCM-22 with a NaOH solution through the protective effect of organic amines such as PI and HMI. This method introduces into the MCM-22 crystals the cylinder-shaped mesopores with a size of around 20 nm. Meanwhile, the 3D structure is converted readily into a 2D layered structure, and the crystallinity of the zeolite is kept intact. The acid sites related to the framework Al are almost not affected by NaOH treatment. Having a larger external surface than MCM-22, meso-MCM-22 is superior to MCM-22 in the cracking of 1,3,5-triisopropylbenzene and the alkylation of benzene with isopropyl alcohol. Thus, meso-MCM-22 zeolites postsynthesized by this method are expected to serve as potential solid acid catalysts for processing bulky molecules.

■ ASSOCIATED CONTENT

Ⓢ Supporting Information

Additional information as noted in text. This material is available free of charge via the Internet at http://pubs.acs.org.

■ AUTHOR INFORMATION

Corresponding Author

*Phone: +86-21-6223-2292. Fax: +86-21-6223-2292. E-mail: pwu@chem.ecnu.edu.cn.

Author Contributions

†Y.-J.J. and H.X. contributed equally.

Notes

The authors declare no competing financial interest.

■ ACKNOWLEDGMENTS

We gratefully acknowledge the National Natural Science Foundation of China (20925310, U1162102), the Ph.D. Programs

Foundation of the Ministry of Education (2012007613000), the Innovation Program of the Shanghai Municipal Education Commission (13zz038), the Key Project of SCST (12JC1403600), the National Key Technology R&D Program (2012BAE05B02), and the Shanghai Leading Academic Discipline Project (B409).

REFERENCES

(1) Rubin, M. K.; Chu, P. U.S. patent 4954325, 1990.
(2) Puppe, L.; Weisser, J. U.S. patent 4439409, 1984.
(3) Zones, S. I.; Holtermann, D. I.; Innes, R. A.; Pecoraro, T. A.; Santilli, D. S.; Ziemer, J. N. U.S. patent 4826667, 1989.
(4) Bellussi, G.; Perego, G.; Clerici, M. G.; Giusti, A. European Patent Application 293032, 1988.
(5) Camblor, M. A.; Corma, A.; Díaz-Cabañas, M.-J.; Baerlocher, C. *J. Phys. Chem. B* **1998**, *102*, 44.
(6) Wu, P.; Komatsu, T.; Yashima, T. *Microporous Mesoporous Mater.* **1998**, *22*, 343.
(7) Perego, C.; Amarilli, S.; Millini, R.; Bellussi, G.; Girotti, G.; Terzoni, G. *Microporous Mater.* **1996**, *6*, 395.
(8) Corma, A.; Martinez-Soria, V.; Schnoeveld, E. *J. Catal.* **2000**, *192*, 163.
(9) Beck, J. S.; Dandekar, A. B.; Degnan, T. F. In *Zeolites for Cleaner Technologies, Catalytic Science Series*; Guisnet, M., Gilson, J.-P., Eds.; Imperial College Press: London, 2002; Vol. 3, p 223.
(10) Chu, C. T. W.; Kresge, C. T.; Roth, W. T.; Simmons, K. G.; Vartuli, J. C. U.S. patent 5292698, 1994.
(11) Roth, W. J.; Kresge, C. T.; Vartuli, J. C.; Leonowicz, M. E.; Fung, A. S.; McCullen, S. B. In *Catalysis by Microporous Materials, Studies in Surface Science and Catalysis*; Beyer, H. K., Karge, H. G., Kiricsi, I., Nagy, J. B., Eds.; Elsevier: Amsterdam, 1995; Vol. 94; p. 301.
(12) Corma, A.; Fornés, V.; Pergher, S. B.; Maessen, T. L. M.; Buglass, J. G. *Nature* **1998**, *396*, 353.
(13) Fung, A. S.; Lawton, S. L.; Roth, J. U.S. patent 5362697, 1994.
(14) Jacobsen, C. J. H.; Madsen, C.; Houzvicka, J.; Schmidt, I.; Carlsson, A. *J. Am. Chem. Soc.* **2000**, *122*, 7116.
(15) Wang, H.; Pinnavaia, T. J. *Angew. Chem., Int. Ed.* **2006**, *45*, 7603.
(16) Groen, J. C.; Peffer, L. A. A.; Moulijn, J. A.; Pérez-Ramírez, J. *Chem.—Eur. J.* **2005**, *11*, 4983.
(17) Meynen, V.; Cool, P.; Vansant, E. F. *Microporous Mesoporous Mater.* **2007**, *104*, 26.
(18) Prokešová, P.; Mintova, S.; Čejka, J.; Bein, T. *Mater. Sci. Eng., C* **2003**, *23*, 1001.
(19) Corma, A.; Díaz-Cabañas, M.-J.; Martínez-Triguero, J.; Rey, F.; Rius, J. *Nature* **2002**, *418*, 514.
(20) Janssen, A. H.; Koster, A. J.; de Jong, K. P. *Angew. Chem., Int. Ed.* **2001**, *40*, 1102.
(21) Groen, J. C.; Jansen, J. C.; Moulijn, J. A.; Pérez-Ramírez, J. *J. Phys. Chem. B* **2004**, *108*, 13062.
(22) Wei, X.; Smirniotis, P. G. *Microporous Mesoporous Mater.* **2006**, *97*, 97.
(23) Groen, J. C.; Sano, T.; Moulijn, J. A.; Pérez-Ramírez, J. *J. Catal.* **2007**, *251*, 21.
(24) Groen, J. C.; Abelló, S.; Villaescusa, L. A.; Pérez-Ramírez, J. *Microporous Mesoporous Mater.* **2008**, *114*, 93.
(25) Pérez-Ramírez, J.; Abelló, S.; Villaescusa, L. A.; Bonilla, A. *Angew. Chem., Int. Ed.* **2008**, *47*, 7913.
(26) Bonilla, A.; Baudouin, D.; Pérez-Ramírez, J. *J. Catal.* **2009**, *265*, 170.
(27) Verboekend, D.; Groen, J. C.; Pérez-Ramírez, J. *Adv. Funct. Mater.* **2010**, *20*, 1441.
(28) Musilová-Pavlačková, Z.; Zones, S. I.; Čejka, J. *Top. Catal.* **2010**, *53*, 273.
(29) Pérez-Ramírez, J.; Verboekend, D.; Bonilla, A.; Abelló, S. *Adv. Funct. Mater.* **2009**, *19*, 3972.
(30) Verboekend, D.; Pérez-Ramírez, J. *Chem.—Eur. J.* **2011**, *17*, 1137.
(31) Li, Y. N.; Liu, S. L.; Zhang, Z. K.; Xie, S. J.; Zhu, X. X.; Xu, L. Y. *Appl. Catal., A* **2008**, *338*, 100.
(32) Srivastava, R.; Choi, M.; Ryoo, R. *Chem. Commun.* **2006**, 4489.
(33) Christensen, C. H.; Johannsen, K.; Schmidt, I.; Christensen, C. H. *J. Am. Chem. Soc.* **2003**, *125*, 13370.
(34) Mei, C. S.; Wen, P. Y.; Liu, Z. C.; Liu, H. X.; Wang, Y. D.; Yang, W. M.; Xie, Z. K.; Hua, W. M.; Gao, Z. *J. Catal.* **2008**, *258*, 243.
(35) Bjørgen, M.; Joensen, F.; Holm, M. S.; Olsbye, U.; Lillerud, K.-P.; Svelle, S. *Appl. Catal., A* **2008**, *345*, 43.
(36) Gopalakrishnan, S.; Zampieri, A.; Schwieger, W. *J. Catal.* **2008**, *260*, 193.
(37) Sun, Y.; Prins, R. *Angew. Chem., Int. Ed.* **2008**, *47*, 8478.
(38) Choi, M.; Cho, H. S.; Srivastava, R.; Venkatesan, C.; Choi, D.-H.; Ryoo, R. *Nat. Mater.* **2006**, *5*, 718.
(39) Liu, K. F.; Xie, S. J.; Xu, G. L.; Li, Y. N.; Liu, S. L.; Xu, L. Y. *Appl. Catal., A* **2010**, *383*, 102.
(40) Liu, K. F.; Xie, S. J.; Liu, S. L.; Xu, G. L.; Gao, N. N.; Xu, L. Y. *J. Catal.* **2011**, *283*, 68.
(41) Camblor, M. A.; Corell, C.; Corma, A.; Díaz-Cabañas, M.-J.; Nicolopoulos, S.; González-Calbet, J. M.; Vallet-Regí, M. *Chem. Mater.* **1996**, *8*, 2415.
(42) Groen, J. C.; Zhu, W. D.; Brouwer, S.; Huynink, S. J.; Kapteijn, F.; Moulijn, J. A.; Pérez-Ramírez, J. *J. Am. Chem. Soc.* **2007**, *129*, 355.
(43) Abelló, S.; Bonilla, A.; Pérez-Ramírez, J. *Appl. Catal., A* **2009**, *364*, 191.
(44) Leonowicz, M. E.; Lawton, J. A. *Science* **1994**, *264*, 5167.
(45) Lawton, J. A.; Lawton, S. L.; Leonowicz, M. E. *Stud. Surf. Sci. Catal.* **1995**, *98*, 250.
(46) Wang, L. L.; Liu, Y. M.; Xie, W.; Wu, H. H.; Li, X. H.; He, M. Y.; Wu, P. *J. Phys. Chem. C* **2008**, *112*, 6132.
(47) Shang, Y. C.; Yang, P. P.; Jia, M. J.; Zhang, W. X.; Wu, T. H. *Catal. Commun.* **2008**, *9*, 907.
(48) Kennedy, G. J.; Lawton, S. L.; Rubin, M. K. *J. Am. Chem. Soc.* **1994**, *116*, 11000.
(49) Hunger, M.; Ernst, S.; Weitkamp, J. *Zeolites* **1995**, *15*, 188.
(50) Kolodziejski, W.; Zicovich-Wilson, C.; Corell, C.; Perez-Pariente, J.; Corma, A. *J. Phys. Chem.* **1995**, *99*, 7002.
(51) Corma, A.; Fornés, V.; Forni, L.; Márquez, F.; Martínez-Triguero, J.; Moscotti, D. *J. Catal.* **1998**, *179*, 451.
(52) Ungureanu, A.; Hoang, T. V.; Trong, On, D.; Dumitriu, E.; Kaliaguine, S. *Appl. Catal., A* **2005**, *294*, 92.
(53) Cheng, M. J.; Tan, D. L.; Liu, X. M.; Han, X. W.; Bao, X. H.; Lin, L. W. *Microporous Mesoporous Mater.* **2001**, *42*, 307.
(54) Namba, S.; Inaka, A.; Yashima, T. *Zeolites* **1986**, *6*, 107.
(55) Namba, S.; Nakanishi, S.; Yashima, T. *J. Catal.* **1984**, *88*, 505.